THE JOURNAL OF PHYSICAL CHEMISTRY C
A JOURNAL OF THE AMERICAN CHEMICAL SOCIETY

pubs.acs.org/JPCC
Article

Covalent Surface Functionalization of Exfoliated MoS_2 Nanosheets for Improved Electrocatalysis

Leandro Hostert, Matheus S. Dias, Caroline B. de Aquino, Felipe C. dos Santos, Valéria S. Marangoni, Cecília de Carvalho C Silva, Leandro Seixas, and Camila M. Maroneze*

Cite This: J. Phys. Chem. C 2024, 128, 20856−20865
Read Online

ABSTRACT: Transition metal dichalcogenides, particularly the metallic phase of molybdenum disulfide (1T'-MoS_2), have attracted significant attention as promising nonprecious metal electrocatalysts for the hydrogen evolution reaction (HER) due to their appealing electrochemical properties and optimal hydrogen adsorption free energy (ΔG_H). In this study, we used a combined theoretical and experimental approach to investigate the covalent functionalization of MoS_2 with $-CH_2COOH$ groups. Notably, the presence of Mo oxidized species(MoO_x) was significantly diminished in the functionalized material, suggesting a potential protective role of the functional groups against MoS_2 oxidation. Additionally, our findings show a decrease in the proportion of the metallic 1T' phase upon functionalization (58% for MoS_2/CH_2COOH compared to 74% for Exf-MoS_2). However, electrochemical measurements unveil a remarkable enhancement in electrocatalytic activity upon the integration of $-CH_2COOH$ groups, as evidenced by observations from Linear Sweep Voltammetry (LSV) and Electrochemical Impedance Spectroscopy (EIS). In LSV analysis, a substantial 53% reduction in the Tafel slope is observed, declining from −145 mV dec^{-1} (for Exf-MoS_2) to −77 mV dec^{-1} (for MoS_2/CH_2COOH). Additionally, EIS measurements indicate a significant decrease in charge transfer resistance, dropping from 82.03 ± 0.11 kΩ/cm^2 (for Exf-MoS_2) to 12.41 ± 0.01 kΩ/cm^2 (for MoS_2/CH_2COOH). The integration of these functional groups onto the MoS_2 surface demonstrates remarkable effectiveness in inhibiting oxidation while concurrently leading to a noteworthy enhancement of catalytic activity for the HER.

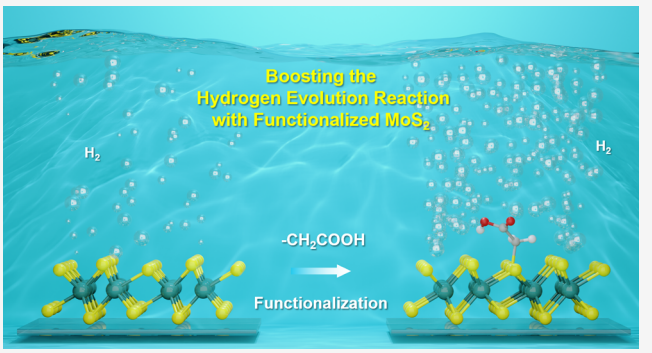

1. INTRODUCTION

The dynamic field of research concerning ultrathin two-dimensional (2D) layered materials consistently reveals that the unique and exceptional properties first observed in graphene are comparably present in other 2D materials,[1] such as transition metal dichalcogenides,[2,3] black phosphorus,[4−6] MXenes,[7] among others. Among these, MoS_2 stands out as an important example, prompting extensive investigations owing to its diverse properties.[8−10] Structural polymorphism in MoS_2 monolayers, resulting from different coordination environments of S atoms around Mo, leads to abrupt changes in electronic properties.[11,12] The 2H-to-1T phase conversion (trigonal prismatic to octahedral structure) is a semiconductor-to-(semi)metal transition that profoundly impacts its applications, particularly in electrochemical technologies.[13,14]

For energy storage and conversion devices, the electrical conductivity of the metallic phases and efficient ion intercalation in layered structures enable the use of MoS_2 as anodes in batteries[15,16] and electrode materials in capacitor devices,[13,17] playing a vital role on the performance. Additionally, electrochemical actuators[18] based on thin films of restacked monolayers of 1T'-MoS_2 (distorted octahedral structure), exhibit the ability to convert electrical energy into mechanical energy. The metallic phase of MoS_2 also exhibits high catalytic activity toward the H_2 evolution reaction (HER) for both edge and basal plane sites,[19−22] making it a promising alternative for clean energy technologies based on hydrogen, which are currently hindered by the high costs of the benchmark Pt-based catalysts. However, the instability of the metastable metallic phases of MoS_2 poses a significant challenge, limiting practical applications and urging the field to address this obstacle.

Surface functionalization of MoS_2 with various species, including metal atoms,[23−25] organic molecules,[26,27] metallic

Received: September 3, 2024
Revised: November 4, 2024
Accepted: November 7, 2024
Published: November 13, 2024

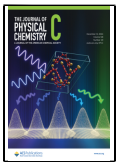

https://doi.org/10.1021/acs.jpcc.4c05965
J. Phys. Chem. C 2024, 128, 20856−20865

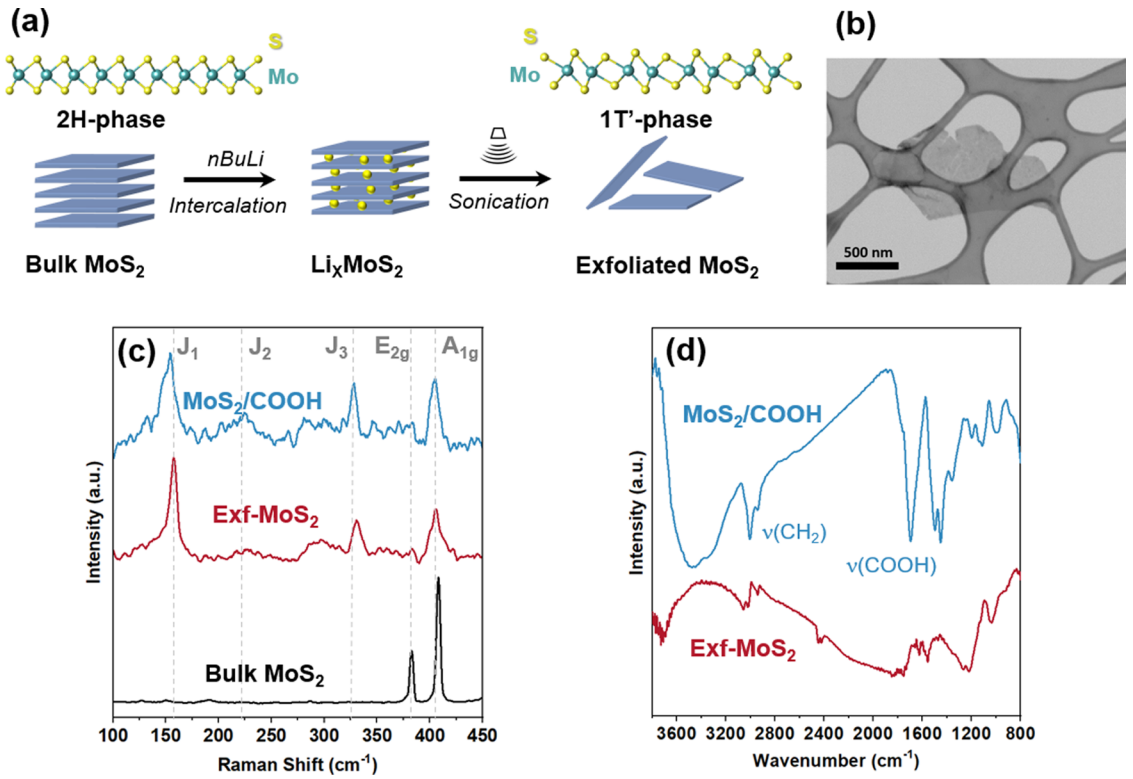

Figure 1. (a) Schematic illustration of the liquid exfoliation of MoS_2 by nBuLi intercalation; (b) scanning transmission electron microscopy (STEM) image of the obtained nanosheets; (c) Raman and (d) Fourier transform infrared (FTIR) spectra for MoS_2 (bulk), Exf-MoS_2, and MoS_2/CH_2COOH samples.

nanoparticles,[28−30] and polymers,[31,32] has been explored as an efficient strategy to modify its intrinsic properties, for multiple purposes and applications, including phase engineering.[33] These functionalized materials have demonstrated improved performance across various fields, from optoelectronic devices[23,34] to catalysis,[26] energy storage/conversion,[35] sensors,[36,37] water purification membranes,[38] and biomedical applications.[39]

In the field of electrocatalysis for H_2 generation, researchers have studied different strategies to functionalize MoS_2 nanosheets to address both phase engineering and catalytic issues. Metal-atom doping of MoS_2 has been extensively studied to tune the electronic states and the adsorption behavior of H atoms on the active sites for the HER, resulting in significant enhancement of the catalytic activity.[25,40−43] Covalent chemical modification using organic phenyl rings, including electron-donating or withdrawing groups, has exhibited enhanced phase stability in the modified samples. Experimental and theoretical findings, derived from density functional theory (DFT) studies of 1T'-MoS_2 functionalized with various molecules (−H, $-CH_3$, $-NO_2Ph$, $-NH_2Ph$, $-CH_2CONH_2$, $-CH_2CH_2OH$), have demonstrated significant improvements in structural stability. However, it was observed that for most functional groups, while structural stability was enhanced, there was a trade-off with compromised electrocatalytic activity. Interestingly, among these groups, those containing electron-donating substituents yielded the most favorable catalytic outcomes.[27] Additionally, there are other factors at play, such as intermolecular forces between the functionalized group and the adsorbed hydrogen, which could modulate the catalytic activity of specific sites, resulting in optimized Gibbs free energy for hydrogen adsorption on the modified surface. This dynamic interaction process may help achieve a good balance between catalytic activity and phase stability.[46,47]

In this study, employing a theoretical-experimental approach, we show how the chemical functionalization of 1T'-MoS_2 with iodoacetic acid molecules improves both the structural stability (phase transition and oxidation) and electrocatalytic properties (surface energetics) of the metallic nanosheets for the HER. The presence of $-CH_2COOH$ groups on the MoS_2 surface enhances the electrocatalytic effects for the HER, reducing the charge transfer resistance at the interface and preventing the oxidation and deactivation of the active sites. We investigate the possible mechanisms involved in stabilization and electrocatalytic effects through first-principles calculations based on DFT, establishing a strong correlation between computational results and experimental findings.

2. EXPERIMENTAL AND THEORETICAL METHODS

2.1. Materials. MoS_2 bulk powder was purchased from Graphene Supermarket and subjected to vacuum drying before utilization. Furthermore, *n*-butyllithium (2.5 M in hexane), hexane (anhydrous, 95%), iodoacetic acid (98%), sulfuric acid (ACS reagent 95−98%), and ITO (indium−tin oxide coated glass slide) were purchased from Sigma-Aldrich. All materials were used as received, except for hexane, which underwent distillation before use.

2.2. Exfoliation of MoS_2. Caution: *n*-butyllithium is highly pyrophoric. MoS_2 nanosheets were exfoliated via the lithium intercalation method,[20] as schematically shown in Figure 1a. Initially, 0.3 g of bulk MoS_2 powder was dispersed and stirred in 4 mL of *n*-butyllithium (2.5 M in hexane) for 1 h under a

https://doi.org/10.1021/acs.jpcc.4c05965
J. Phys. Chem. C 2024, 128, 20856−20865

nitrogen atmosphere. Subsequently, 10 mL of anhydrous hexane was added to the system and refluxed for 48 h at 70 °C. The MoS_2 suspension was then subjected to centrifugation (2000 rpm for 5 min) and washed twice with hexane. The lithium-intercalated MoS_2 was then dispersed in deionized water at 1.5 mg mL^{-1}, sonicated for 1 h, and centrifuged at 4000 rpm for 30 min to remove the nonexfoliated MoS_2. Finally, the supernatant was recovered and purified using a dialysis membrane (porosity of 12 kDa) in deionized water.

2.3. Functionalization of the MoS_2 Nanosheets. Exfoliated MoS_2 nanosheets were functionalized using iodoacetic acid molecules.[48] 50 mL of the aqueous dispersion of exfoliated MoS_2 was diluted to 100 mL with deionized water, and 2.0×10^{-4} mol of the functionalizing agent (iodoacetic acid) was added. After 5 days of reaction at room temperature, the material was washed with deionized water (2×50 mL) via centrifugation.

2.4. Characterization. The concentrations of the purified MoS_2 and MoS_2/CH_2COOH suspensions were determined by Atomic Absorption Spectrometry (contrAA 800 D Atomic Absorption Spectrometry System from Analytik Jena). Raman spectroscopy analysis was conducted using the Witec confocal spectrometer model UHTS 300 (532 nm, 0.3 mW) with a 50× magnification objective lens for all measurements. Samples were drop cast on Si/SiO_2 substrates. FT-IR spectra were obtained on an IRAffinity-1 SHIMADZU, equipped with ATR (PIKE Technologies) accessory. The spectra were collected by pressing the sample onto a diamond crystal. Each spectrum consisted of 16 spectra coadded and accumulated between 4000 and 600 cm^{-1}. Zeta potential measurements were conducted using a Particle Analyzer Model Litesizer 500 Anton Paar. The morphology of the resulting exfoliated MoS_2 was investigated via Scanning Transmission Electron Microscopy (STEM) using a FEI Inspect F50 microscope operating at 30 kV. The sample was deposited on Lacey Carbon TEM grids (TedPella). X-ray Photoelectron Spectroscopy (XPS) analysis was performed using a commercial UNI-SPECS UHV spectrometer with base pressure below 5×10^{-7} Pa. The Mg Kα line was used ($h\nu$ = 1253.6 eV) as the ionization source and the pass energy of the analyzer was adjusted to 10 eV. The high-resolution Mo 3d spectra underwent inelastic noise subtraction using Shirley's method. The binding energy of the spectra was corrected using the hydrocarbon component fixed at 284.9 eV. The spectra were deconvolved using a Pseudo-Voigt function, with Gaussian (70%) and Lorentzian (30%) combinations. The width at half height varied between 1.2 and 2.1 eV, and the position of the peaks was determined with an accuracy of ±0.1 eV.

2.5. Electrochemical Measurements. Electrochemical measurements were conducted using a three-electrode cell, employing a Metrohm Autolab Potentiostat (PGSTAT204). Graphite rods and Ag/AgCl (3 M KCl) were used as counter and reference electrodes, respectively. Working electrodes were prepared by drop casting 3 μL of the Exf-MoS_2 or MoS_2/CH_2COOH suspension (0.1 mg/mL) on indium-doped tin oxide (ITO) coated glass slides within a limited area of 0.080 cm^{-2}. All the measurements were performed in an aqueous H_2SO_4 (0.5 M) electrolyte deaerated with nitrogen gas. Linear sweep voltammetry was conducted at a 10 mV s^{-1} scan rate in the interval between −0.1 and −0.5 V vs RHE. Electrochemical impedance spectroscopy (EIS) studies were carried out across a frequency range spanning from 1 MHz down to 0.1 Hz. These measurements were performed with a root-mean-square amplitude of 10 mV, maintaining a fixed bias potential at −0.30 V vs RHE. The electrochemical active surface area (ESCA) was determined by the capacitive current method[49] in KCl 0.1 M at scan rates varying from 5 to 100 mV s^{-1}. The ESCA values were 0.10 and 0.09 cm^2 for the Exf-MoS_2 and MoS_2/CH_2COOH electrodes, respectively. These values were used for the normalized cathodic polarization curves (LSV) plots.

2.6. *Ab Initio* Simulations. Simulations were conducted utilizing density functional theory (DFT).[50,51] The GPAW code[52] was applied, utilizing a plane wave basis[53] and setting the cutoff energy at 500 eV for all studies. The projector augmented wave method (PAW)[54] was used to determine the external potential, while the exchange-correlation effects were addressed using the generalized gradient approximation as defined by Perdew−Burke−Ernzerhof (PBE).[55] Additionally, van der Waals (vdW) interactions were accounted for using the DFTD4 method,[56,57] aiding in total energy calculations and geometry optimizations. The *k*-point sampling was executed via the Monkhorst−Pack scheme,[58] selecting grids of $5 \times 5 \times 1$ for 2H-MoS_2 and $9 \times 5 \times 1$ for 1T'-MoS_2. To eliminate unwanted interactions, a vacuum spacing of 10 Å was maintained. Geometry optimization was conducted until the force fell below 0.01 eV $Å^{-1}$. For processes like covalent functionalization, oxidation, and hydrogen adsorption, 3×2 orthorhombic supercells were employed with a *k*-point grid of $3 \times 3 \times 1$.

The formation energy of covalent functionalizations is given by

$$\Delta E^{f}(MoS_2 + X) = E_{tot}(MoS_2 + X) - E_{tot}(MoS_2) - E_{tot}(XI) + \mu_I \quad (1)$$

where X = CH_2COOH, E_{tot} is the total energy and $\mu_I = E_{tot}(HI) - \frac{1}{2}E_{tot}(H_2)$ is the chemical potential of iodine.

For the study of oxidation processes, the formation energy is calculated by

$$\Delta E^{f}(MoS_2 + 2O^*) = E_{tot}(MoS_2 + 2O^*) - E_{tot}(MoS_2 + O_2) \quad (2)$$

Here, $E_{tot}(MoS_2 + 2O^*)$ is the total energy of MoS_2 with two oxygen atoms chemically adsorbed and $E_{tot}(MoS_2 + O_2)$ is the total energy of MoS_2 with the O_2 molecule physically adsorbed.

The Gibbs free energy for hydrogen adsorption, a key theoretical descriptor for evaluating the catalysis of the hydrogen evolution reaction, is determined by

$$\Delta G_H = \Delta E_H + \Delta E_{ZPE} - T\Delta S_H \quad (3)$$

Here,

$$\Delta E_H = E_{tot}(MoS_2 + H^*) - E_{tot}(MoS_2) - \frac{1}{2}E_{tot}(H_2) \quad (4)$$

represents the hydrogen adsorption energy on MoS_2 (a semiclassical approximation), ΔE_{ZPE} is the variation of zero-point energy (first-order quantum correction) and ΔS_H denotes the entropy change between adsorbed hydrogen (H*) and H_2 gas. We employ the Nørskov approximation in this study,[59] which simplifies the Gibbs free energy calculation to

https://doi.org/10.1021/acs.jpcc.4c05965
J. Phys. Chem. C 2024, 128, 20856−20865

$$\Delta G_H = \Delta E_H + 0.24\ \text{eV} \quad (5)$$

3. RESULTS AND DISCUSSION

The covalent modification of the MoS_2 surface was performed on the MoS_2 nanosheets previously exfoliated using the Li intercalation method (Figure 1a). This process primarily yields dispersed monolayers and/or ultrafine MoS_2, as illustrated in the STEM image (Figure 1b). The nanosheets exhibit lateral dimensions in the range of 500−1000 nm and the typical morphology of chemically exfoliated MoS_2.[60] The chemical exfoliation via Li intercalation is known to induce the phase transition from the semiconducting 2H to the metallic 1T' phase,[8,61] as observed in the Raman spectra (Figure 1c). The bulk 2H-MoS_2 is identifiable by the E_{2g} and A_{1g} modes at 383 and 409 cm^{-1}, respectively. In contrast, the exfoliated material (Exf-MoS_2) shows a significant decrease in the E_{2g} signal and the emergence of the J_1 (157 cm^{-1}), J_2 (223 cm^{-1}), and J_3 (330 cm^{-1}) modes, associated with the 1T'-MoS_2 metallic phase.[62] The 2H-to-1T' phase transition is attributed to the electron transfer from Li during the intercalation process, destabilizing the trigonal prismatic structure (2H) and favoring the distorted octahedral structure (1T').[8,63]

The covalent functionalization of the metallic nanosheets (Exf-MoS_2) was confirmed via attenuated total reflectance Fourier-transformed infrared spectroscopy (ATR-FTIR)-(Figure 1d). Bands at ≈3400 cm^{-1} (νOH), 2974 and 2905 cm^{-1} (νCH_2), 1700 cm^{-1} (νCOOH), and ≈1420 cm^{-1} ($\nu C{=}O$) indicate the presence of the organic molecules in the functionalized MoS_2/CH_2COOH material.[64] Notably, the zeta potential of the MoS_2/CH_2COOH aqueous suspension (−32.3 mV) became less negative after the functionalization reaction compared to the Exf-MoS_2 (−41.5 mV), suggesting the suppression of negative charges on the MoS_2 nanosheets and the attachment of functional groups.[65] The pH values of the Exf-MoS_2 and MoS_2/CH_2COOH aqueous suspensions, 7.8 and 4.4 respectively, also corroborate with the presence of acid groups on the surface of the functionalized material. Importantly, the 1T' phase is well preserved in the functionalized material (MoS_2/CH_2COOH), as observed by the presence of the J modes in the Raman spectrum (Figure 1c). The X-ray diffraction patterns of the MoS_2 (bulk), the exfoliated (Exf-MoS_2) nanosheets and the functionalized material (MoS_2/CH_2COOH) show the expected shift of the (002) peak to lower angles the exfoliation and functionalization (Figure S1). These shifts are associated with an increased interlayer spacing, resulting from the random restacking of the exfoliated MoS_2 nanosheets and the presence of grafted functional groups.

To elucidate the position of the functional groups on the MoS_2 nanosheets, DFT calculations were performed. The formation energies for the functionalization reaction on distinct sites of the metallic 1T'-MoS_2 (Figure 2a) are schematically shown in the energy diagram, presented in Figure 2b. The calculated values indicate that the organic groups must be preferentially bond to the S atoms in the S_L position (Figure 2a), with the formation energy $\Delta E_L^f = -0.33$ eV. This site is favored over the S_H position that shows ΔE_H^f = 0.05 eV. The formation energy for the functionalization of the S sites on the 2H phase was also calculated (Figure 2c), with ΔE_{2H}^f = 1.37 eV. The positive value substantiates the experimentally observed nonspontaneous nature of the reaction between 2H-MoS_2 and organohalides.[48]

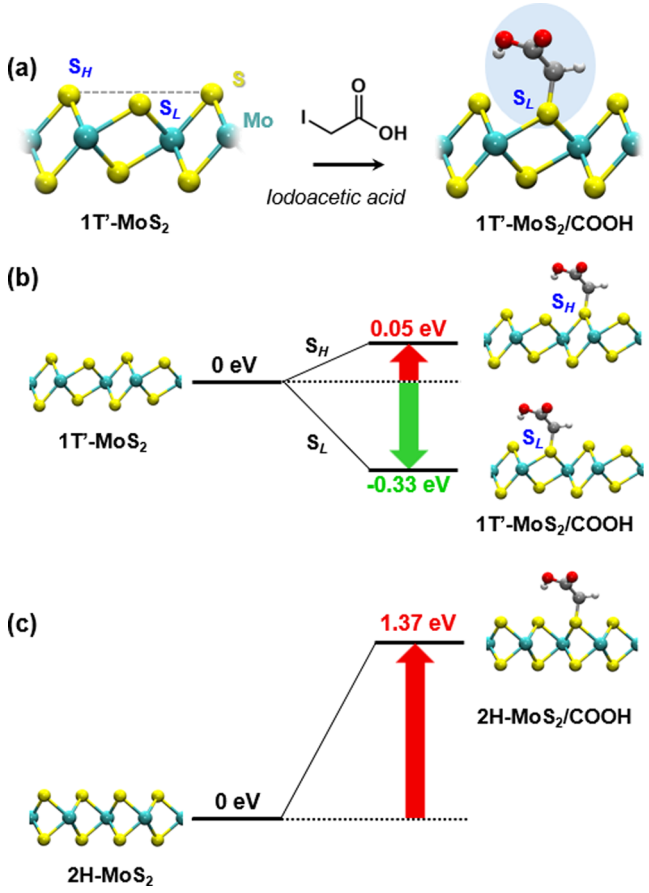

Figure 2. (a) Schematic reaction for the covalent functionalization of 1T'-MoS_2 with iodoacetic acid. Energy diagram with the functionalization formation energies (ΔE^f) for distinct S sites of (b) 1T'-MoS_2 and (c) 2H-MoS_2.

To understand how functional groups affect the structural integrity and oxidation resistance of 1T'-MoS_2, DFT calculations were conducted. As can be observed in Figure 3a,b, the presence of the functional groups ($-CH_2COOH$) on the MoS_2 surface decreases its susceptibility to oxidation. The formation energy for the oxidation of the functionalized 1T'-MoS_2/CH_2COOH (ΔE^f = −1.46 eV) is less negative than the pristine 1T'-MoS_2 (ΔE^f = −1.59 eV). The long-term stability of the samples was monitored by Raman spectroscopy (Figure S2) and corroborates with the DFT calculations concerning the susceptibility to oxidation and the 1T'-to-2H phase conversion, with higher stability for the functionalized MoS_2. This is crucial as oxidation can significantly deteriorate the electrocatalytic performance of metallic MoS_2 for the HER by altering the active sites and the optimal hydrogen adsorption energies (ΔG_H). Such deterioration can occur by the formation of less conductive or even insulating layers on the surface and also by promoting the 1T'-to-2H phase transformation, diminishing the material's overall catalytic activity.

XPS spectra (Mo 3d) for Exf-MoS_2 and MoS_2/CH_2COOH samples (Figure 3c,d) provide important additional information concerning the structural properties. The samples exhibit a mixed-phase character (1T'/2H), with the 1T' metallic phase (Mo $3d_{5/2}$ ≈ 228.4 eV and Mo $3d_{3/2}$ ≈ 231.5 eV) predominantly present both in the pristine and the functionalized material. The 1T' phase proportions were found to be 74 and 58% for Exf-MoS_2 and MoS_2/CH_2COOH, respectively.

https://doi.org/10.1021/acs.jpcc.4c05965
J. Phys. Chem. C 2024, 128, 20856−20865

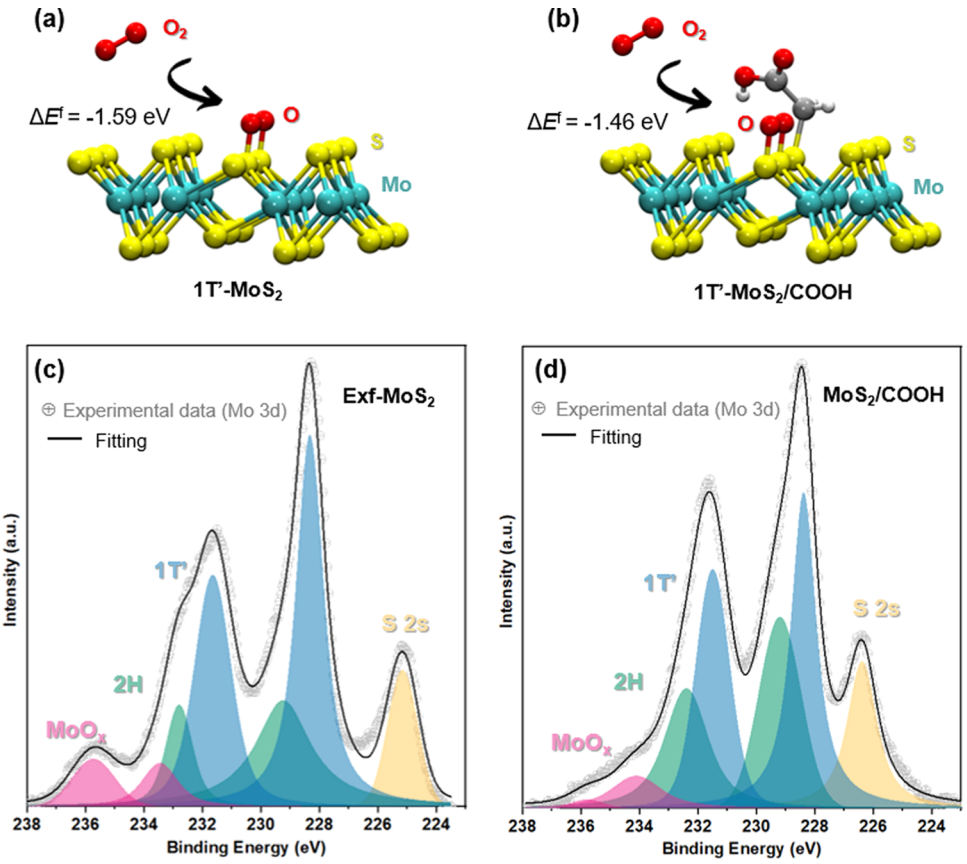

Figure 3. Schematic illustrations of the oxidation sites and their respective formation energies on the surface of the (a) pristine 1T'-MoS_2 and (b) functionalized 1T'-MoS_2/CH_2COOH materials. High-resolution XPS spectra (Mo 3d) of the (c) Exf-MoS_2 and (d) MoS_2/CH_2COOH samples.

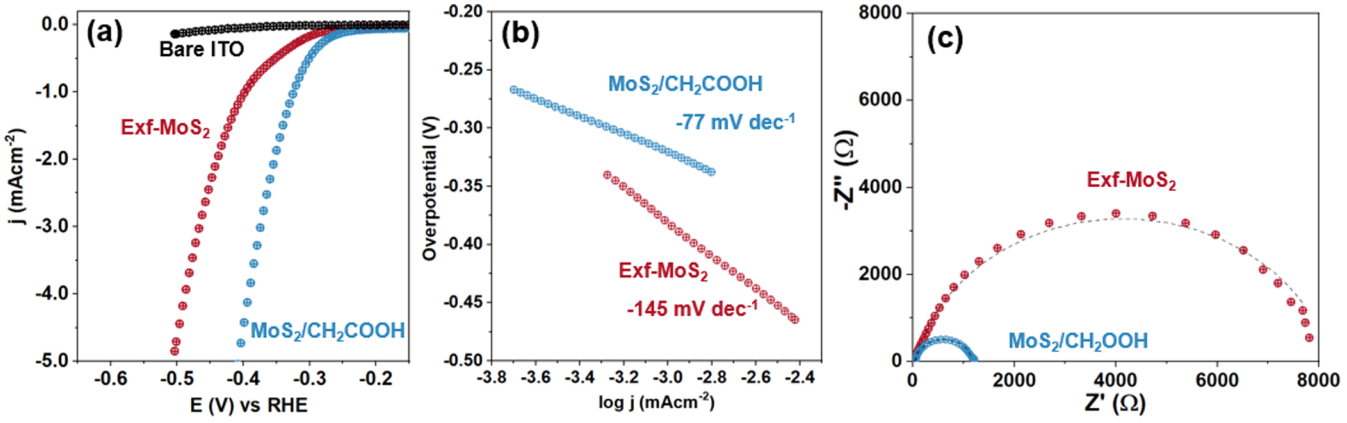

Figure 4. (a) Cathodic polarization curves obtained at scan rate of 10 mV s^{-1} in 0.5 M H_2SO_4 and the corresponding (b) Tafel plots for the Exf-MoS_2 and MoS_2/CH_2COOH samples. (c) Electrochemical impedance spectroscopy (Nyquist plots) for the Exf-MoS_2 and MoS_2/CH_2COOH samples and the respective fitted curves (dashed lines). All the spectra were collected by scanning from 0.1 to 10 MHz in a fixed bias of −0.3 V vs RHE.

After the functionalization reaction, the 1T'-phase concentration is partially reduced, likely due to the suppression of excess charge caused by the attachment of functional groups, which can induce 1T'-to-2H phase conversion. Thermogravimetric analysis (TGA) was carried out to evaluate the surface modification with the functional groups and is shown in the Figure S3. The reduction of negative charges on the nanosheets after the functionalization reaction was confirmed by the zeta potential values discussed before. The S 2p XPS spectra for the Exf-MoS_2 and MoS_2/CH_2COOH (Figure S4) show a small shift after the functionalization, also indicating the covalent surface modification.

Additionally, the oxidation process was investigated through XPS measurements (Figure 3c,d) by the Mo peaks at binding energies of ≈235.7 and ≈233.5 eV, attributed to Mo^{VI} and Mo^{V} species (MoO_x). Notably, the samples (aqueous suspensions) were stored under consistent conditions (30 days in the refrigerator at +5 °C followed by 15 days on the Si/SiO_2 substrate as a thin film at ambient conditions) before the measurements. The spectra indicate a significantly lower

https://doi.org/10.1021/acs.jpcc.4c05965
J. Phys. Chem. C 2024, 128, 20856−20865

formation of Mo oxidized species (MoO_x) in the functionalized material, suggesting that the functional groups may play a protective role in preventing the oxidation of the MoS_2 structure. These experimental observations show a strong correlation with the DFT simulations presented earlier.

It is worth mentioning that while the functional groups on the surface of MoS_2 prevent oxidation, they could potentially hinder the reactivity of sulfur sites for the hydrogen evolution reaction. However, the surface S atoms remain partially passivated, with unmodified sites available for hydrogen adsorption. To comprehend how functional groups impact surface catalysis, electrocatalytic HER performance was evaluated for both pristine and modified MoS_2 samples using a three-electrode cell in 0.5 M H_2SO_4 electrolyte solution. Figure 4 shows representative linear sweep voltammograms (LSV) for the ITO substrate, Exf-MoS_2, and MoS_2/CH_2COOH. Initially, the ITO exhibits minimal activity for the HER and is expected to have a negligible effect on the overall reduction process. Comparative analysis between the pristine Exf-MoS_2 and the functionalized MoS_2/CH_2COOH clearly shows an increase in the electrocatalytic activity for the functionalized material (MoS_2/CH_2COOH), evidenced by the current density curve profiles and the decrease of the overpotential at 5 mA cm^{-2} for the MoS_2/CH_2COOH compared to the pristine Exf-MoS_2, respectively −0.41 and −0.51 V vs RHE. Corresponding Tafel plots (Figure 4b) illustrate a significant decrease in the Tafel slope from −145 to −77 mV dec^{-1}, affirming the beneficial role of the functional groups in improving the electrocatalytic activity of the MoS_2 material. The decrease in the Tafel slope suggests that the probable reaction mechanism (Volmer−Heyrovsky) might be transitioning from a rate-determining step (RSD) where the availability and adsorption of hydrogen species is critical (Volmer for the pristine Exf-MoS_2) to an RSD where the primary challenge shifts to the desorption of H_2 (Heyrovsky for the MoS_2/CH_2COOH).[66] These results highlight the role played by the $-CH_2COOH$ groups on the energetics of hydrogen adsorption but also indicate the possibility of other additional effects inside the electrochemical double layer (EDL), like the hydrogen-bond networks, further discussed. This observation is surprising considering that the surface S atoms are not completely passivated, although the functional groups present on the MoS_2 surface could impede the activity of certain sulfur sites in the HER. Further evaluation of the superior performance of functionalized MoS_2/CH_2COOH was conducted through EIS to assess the electrode kinetics under HER operating conditions. Nyquist plots for the Exf-MoS_2 and the MoS_2/CH_2COOH samples (at −0.30 V vs RHE) are shown in (Figure 4c). The equivalent circuit used to fit the EIS data and the values of the parameters are shown in the (Figure S5 and Table S1). The charge transfer resistance (R_{CT}) values determined for the pristine Exf-MoS_2 and functionalized MoS_2/CH_2COOH are ≈82.03 ± 0.11 and ≈12.41 ± 0.01 kΩ/cm^2, respectively. The substantial decrease in charge transfer resistance for the modified material corroborates with the improved electrocatalytic performance observed previously through linear sweep voltammetry.

Analyzing the 1T'/2H ratio in both materials reveals a lower proportion of the 1T' phase in the functionalized material (58 vs 74% for the Exf-MoS_2), suggesting it may not exhibit superior catalytic performance, considering electronic transport and the conductivity of MoS_2 nanosheets. Furthermore, catalysis might be adversely affected by functional groups partially occupying some active sites on the surface. Nevertheless, it becomes evident that the influence of functional groups overcomes these limitations, potentially improving the HER.

To enhance our understanding of the significant impact that functional groups have on catalytic behavior, we also evaluated the hydrogen adsorption process using DFT calculations. The Gibbs free energy for hydrogen adsorption at the main sulfur sites in both pristine and functionalized materials is depicted in Figure 5a,b. The protonated form of the functional groups was used in the DFT calculations considering the experimental conditions carried out for HER (Table S2).

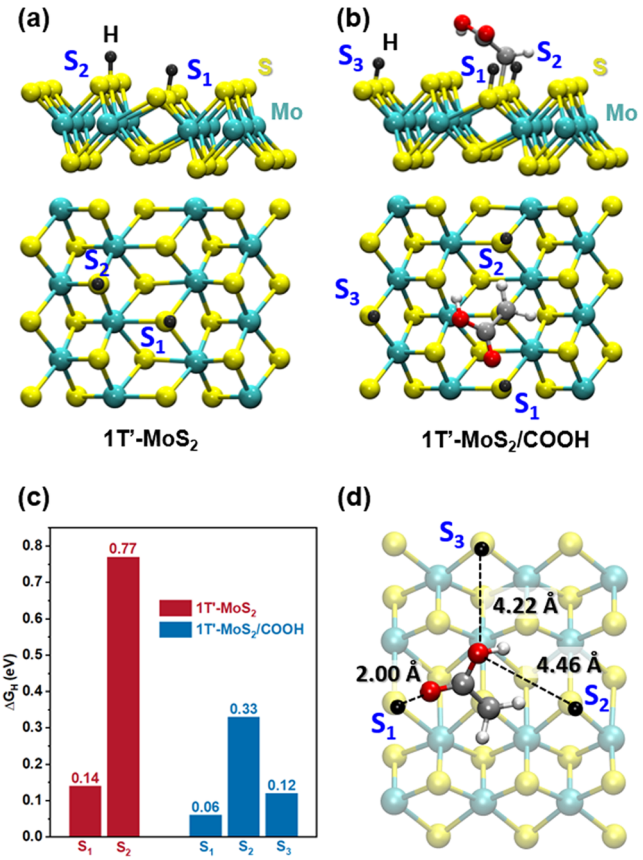

Figure 5. Schematic illustrations of the S catalytic sites for H adsorption (lateral and top views) on the surface of the (a) pristine 1T'-MoS_2 and (b) functionalized 1T'-MoS_2/CH_2COOH materials; (c) The Gibbs free energy for hydrogen adsorption on different S sites of the pristine 1T'-MoS_2 and 1T'-MoS_2/CH_2COOH materials; (d) Geometry of H adsorption with the H···O distances on the functionalized 1T'-MoS_2.

For the pristine material, positions S_1 and S_2 (Figure 5a), equivalent to previously discussed S_L and S_H sites, exhibit ΔG_H values of 0.14 and 0.77 eV, respectively (Figure 5c). Similar to the functionalization process, the S_1 (S_L) site proves to be more active for the HER, with its ΔG_H value closer to zero. In the case of the functionalized material, we assessed three different sites associated with the sulfur atom in the more reactive S_L position, surrounding the functional group (Figure 5b). The calculated ΔG_H for the S_1, S_2, and S_3 sites are 0.06, 0.33, and 0.12 eV respectively. These values show a notable increase in catalytic activity for the functionalized MoS_2 at the S_1 position compared to the sites of the unmodified material,

https://doi.org/10.1021/acs.jpcc.4c05965
J. Phys. Chem. C 2024, 128, 20856−20865

and a slight improvement for the S_3 site. The S_2 site is the least active (ΔG_H = 0.33 eV) among them, suggesting a possible effect of the distance between the catalytic site and the functional group. To comprehend the observed variation, we examined the bonding structures related to hydrogen adsorption (Figure 5d). Specifically, at site S_1, a distinctive hydrogen bond interaction is noted between the adsorbed hydrogen and the carbonyl oxygen in the $-CH_2COOH$ group, characterized by an H···O distance of 2.00 Å. For the sites S_2 and S_3, the hydrogen bonding formation may not be present due to the longer H···O distances (4.46 and 4.22 Å respectively). In addition to the effects related to the ΔG_H, which clearly indicated that the functional groups promoted an optimization on the binding energies of the reactive intermediates, with significant changes in Tafel slopes, the possibility of hydrogen-bond (HB) networks within the electric double layer (EDL) may cause additional kinetic effects. The $-CH_2COOH$ groups attached to the surface could strengthen the HB networks by acting as additional HB donors within the EDL, potentially stabilizing intermediates and reducing the kinetic barrier of the HER. This could facilitate proton transfer in the Volmer step, promoting faster reaction rates through an effectively "structured" water environment. This phenomenon has been observed and reported for Pt catalyst and attributed to an increased connectivity of hydrogen-bond networks in the EDL.[67] The hydrogen bond formation seems to play a significant role in optimizing the energetics for hydrogen adsorption and boosting the HER activity, offering valuable insights for the practical design of effective MoS_2-based electrocatalysts for hydrogen production.

4. CONCLUSIONS

In summary, our theoretical-experimental approach has highlighted the beneficial role of covalent functionalization of metallic 1T'-MoS_2 nanosheets with $-CH_2COOH$ groups for the HER. We have observed that these functional groups on the surface can protect the metastable 1T'-MoS_2 from oxidation, thus preventing passivation and/or deactivation of the catalytic sites on the surface. Although the functionalized sample shows a decreased proportion of the metallic 1T' phase (58% for MoS_2/CH_2COOH compared to 74% for Exf-MoS_2), which would typically suggest reduced HER activity, our results demonstrate enhanced catalytic performance due to the presence of the functional groups. Specifically, the $-CH_2COOH$ groups modify the active sites and surface chemistry of MoS_2, effectively compensating for the lower metallic 1T' phase proportion and leading to improved overall catalytic activity. This enhancement is evident through two key measurements: LSV and EIS. In LSV analysis, there is a notable 53% reduction in the Tafel slope, decreasing from -145 mV dec^{-1} (for Exf-MoS_2) to -77 mV dec^{-1} (for MoS_2/CH_2COOH). Additionally, EIS measurements indicate a substantial decrease in charge transfer resistance (R_{CT}), dropping from 82.03 ± 0.11 kΩ/cm^2 (for Exf-MoS_2) to 12.41 ± 0.01 kΩ/cm^2 (for MoS_2/CH_2COOH). DFT calculations have been conducted to understand these unexpected experimental observations, and the ΔG_H values for different S sites surrounding the functional group clarify the substantial enhancement achieved, despite possible disadvantages regarding the blocking of active sites and the 1T'-to-2H phase conversion during functionalization. Consequently, despite the lower proportion of the metallic phase, the inclusion of $-CH_2COOH$ groups in 1T'-MoS_2 substantially enhances its electrocatalytic activity, positioning this material as a promising catalyst with enhanced stability for the HER.

ASSOCIATED CONTENT

Supporting Information

The Supporting Information is available free of charge at https://pubs.acs.org/doi/10.1021/acs.jpcc.4c05965.

X-ray diffraction characterization; long-term stability of the samples monitored by Raman spectroscopy; thermogravimetric analysis (TGA); X-ray photoelectron spectroscopy (XPS); electrochemical impedance spectroscopy (EIS); zeta potential (PDF)

AUTHOR INFORMATION

Corresponding Author

Camila M. Maroneze − *School of Engineering, Mackenzie Presbyterian University, São Paulo - SP 01302-907, Brazil; MackGraphe - Mackenzie Institute for Research in Graphene and Nanotechnologies, Mackenzie Presbyterian Institute, São Paulo - SP 01302-907, Brazil;* orcid.org/0000-0002-6835-4476; Email: camila.maroneze@mackenzie.br

Authors

Leandro Hostert − *School of Engineering, Mackenzie Presbyterian University, São Paulo - SP 01302-907, Brazil; MackGraphe - Mackenzie Institute for Research in Graphene and Nanotechnologies, Mackenzie Presbyterian Institute, São Paulo - SP 01302-907, Brazil*

Matheus S. Dias − *School of Engineering, Mackenzie Presbyterian University, São Paulo - SP 01302-907, Brazil; MackGraphe - Mackenzie Institute for Research in Graphene and Nanotechnologies, Mackenzie Presbyterian Institute, São Paulo - SP 01302-907, Brazil*

Caroline B. de Aquino − *School of Engineering, Mackenzie Presbyterian University, São Paulo - SP 01302-907, Brazil; MackGraphe - Mackenzie Institute for Research in Graphene and Nanotechnologies, Mackenzie Presbyterian Institute, São Paulo - SP 01302-907, Brazil*

Felipe C. dos Santos − *School of Engineering, Mackenzie Presbyterian University, São Paulo - SP 01302-907, Brazil; MackGraphe - Mackenzie Institute for Research in Graphene and Nanotechnologies, Mackenzie Presbyterian Institute, São Paulo - SP 01302-907, Brazil*

Valéria S. Marangoni − *School of Engineering, Mackenzie Presbyterian University, São Paulo - SP 01302-907, Brazil; MackGraphe - Mackenzie Institute for Research in Graphene and Nanotechnologies, Mackenzie Presbyterian Institute, São Paulo - SP 01302-907, Brazil; Ilum School of Science, Brazilian Center for Research in Energy and Materials (CNPEM), Campinas - SP 13087-548, Brazil;* orcid.org/0000-0002-3732-504X

Cecília de Carvalho C Silva − *School of Engineering, Mackenzie Presbyterian University, São Paulo - SP 01302-907, Brazil; MackGraphe - Mackenzie Institute for Research in Graphene and Nanotechnologies, Mackenzie Presbyterian Institute, São Paulo - SP 01302-907, Brazil;* orcid.org/0000-0003-3933-1838

Leandro Seixas − *School of Engineering, Mackenzie Presbyterian University, São Paulo - SP 01302-907, Brazil; MackGraphe - Mackenzie Institute for Research in Graphene and Nanotechnologies, Mackenzie Presbyterian Institute, São*

Paulo - SP 01302-907, Brazil; orcid.org/0000-0001-7420-0708

Complete contact information is available at: https://pubs.acs.org/10.1021/acs.jpcc.4c05965

Author Contributions

L.H.: Formal analysis, Data curation, Methodology, Writing—original draft. M.S.D.: Methodology and Data curation. C.B.d.A.: Formal analysis, Data curation, Methodology. F.C.d.S.: Formal analysis, Data curation, Methodology. V.S.M. Formal analysis, Data curation, Methodology, Investigation. C.d.C.C.S.: Formal analysis, Investigation. L.S.: Formal analysis, Data curation, Investigation, Methodology. C.M.M.: Conceptualization, Formal analysis, Funding acquisition, Investigation, Methodology, Project administration, Resources, Validation, Writing—review and editing.

Funding

The Article Processing Charge for the publication of this research was funded by the Coordination for the Improvement of Higher Education Personnel - CAPES (ROR identifier: 00x0ma614).

Notes

The authors declare no competing financial interest.

■ ACKNOWLEDGMENTS

The authors acknowledge financial support from the Fundo Mackenzie de Pesquisa e Inovação (MackPesquisa), Coordenação de Aperfeiçoamento de Pessoal de Nível Superior (CAPES), Conselho Nacional de Desenvolvimento Científico e Tecnológico (CNPq) (Grants Nos. 311324/2020-7, 408248/2023-8, 313091/2022-6), INCT Materials Informatics (Grant No. 406447/2022-5), INCT NanoVida (Grant No. 406079/2022-6), Financiadora de Estudos e Projetos (FINEP, Grant No. 1151/22) and Fundação de Amparo a Pesquisa do Estado de São Paulo (FAPESP) (Grants No. 2022/14549-3, 2016/20799-1). The authors also thank the Centro Nacional de Processamento de Alto Desempenho em São Paulo (CENAPAD-SP) for providing computational facilities and CNPEM-LNNano for the STEM measurements.

■ REFERENCES

(1) Tan, C.; Cao, X.; Wu, X.-J.; He, Q.; Yang, J.; Zhang, X.; Chen, J.; Zhao, W.; Han, S.; Nam, G.-H.; et al. Recent advances in ultrathin two-dimensional nanomaterials. *Chem. Rev.* **2017**, *117*, 6225−6331.

(2) Zhou, J.; Lin, J.; Huang, X.; Zhou, Y.; Chen, Y.; Xia, J.; Wang, H.; Xie, Y.; Yu, H.; Lei, J.; et al. A library of atomically thin metal chalcogenides. *Nature* **2018**, *556*, 355−359.

(3) Manzeli, S.; Ovchinnikov, D.; Pasquier, D.; Yazyev, O. V.; Kis, A. 2D transition metal dichalcogenides. *Nat. Rev. Mater.* **2017**, *2*, No. 17033.

(4) Castellanos-Gomez, A. Black Phosphorus: Narrow Gap, Wide Applications. *J. Phys. Chem. Lett.* **2015**, *6*, 4280−4291.

(5) Xia, F.; Wang, H.; Hwang, J. C.; Neto, A. H.; Yang, L. Black phosphorus and its isoelectronic materials. *Nature Reviews Physics* **2019**, *1*, 306−317.

(6) Marangoni, V. S.; Cadore, A. R.; Ribeiro, H. B.; Hostert, L.; de Matos, C. J.; Silva, C. C.; Seixas, L.; Maroneze, C. M. Long-term environmental stability of nitrogen-healed black phosphorus. *Appl. Surf. Sci.* **2021**, *564*, No. 150450.

(7) Gogotsi, Y.; Anasori, B. The Rise of MXenes. *ACS Nano* **2019**, *13*, 8491−8494.

(8) Chhowalla, M.; Shin, H. S.; Eda, G.; Li, L.-J.; Loh, K. P.; Zhang, H. The chemistry of two-dimensional layered transition metal dichalcogenide nanosheets. *Nat. Chem.* **2013**, *5*, 263−275.

(9) Huang, X.; Zeng, Z.; Zhang, H. Metal dichalcogenide nanosheets: Preparation, properties and applications. *Chem. Soc. Rev.* **2013**, *42*, 1934−1946.

(10) Hinnemann, B.; Moses, P. G.; Bonde, J.; Jørgensen, K. P.; Nielsen, J. H.; Horch, S.; Chorkendorff, I.; Nørskov, J. K. Biomimetic hydrogen evolution: MoS2 nanoparticles as catalyst for hydrogen evolution. *J. Am. Chem. Soc.* **2005**, *127*, 5308−5309.

(11) Chhowalla, M.; Shin, H. S.; Eda, G.; Li, L. J.; Loh, K. P.; Zhang, H. The chemistry of two-dimensional layered transition metal dichalcogenide nanosheets. *Nat. Chem.* **2013**, *5*, 263−275.

(12) Yang, H.; Kim, S. W.; Chhowalla, M.; Lee, Y. H. Structural and quantum-state phase transitions in van der Waals layered materials. *Nat. Phys.* **2017**, *13*, 931−937.

(13) Wang, T.; Chen, S.; Pang, H.; Xue, H.; Yu, Y. MoS2-Based Nanocomposites for Electrochemical Energy Storage. *Adv. Sci.* **2017**, *4* (2), No. 1600289.

(14) Pumera, M.; Sofer, Z.; Ambrosi, A. Layered transition metal dichalcogenides for electrochemical energy generation and storage. *J. Mater. Chem. A* **2014**, *2*, 8981−8987.

(15) Lei, Z.; Zhan, J.; Tang, L.; Zhang, Y.; Wang, Y. Recent Development of Metallic (1T) Phase of Molybdenum Disulfide for Energy Conversion and Storage. *Adv. Energy Mater.* **2018**, *8* (19), No. 1703482.

(16) Wu, M.; Zhan, J.; Wu, K.; Li, Z.; Wang, L.; Geng, B.; Wang, L.; Pan, D. Metallic 1T MoS2 nanosheet arrays vertically grown on activated carbon fiber cloth for enhanced Li-ion storage performance. *J. Mater. Chem. A* **2017**, *5*, 14061−14069.

(17) Acerce, M.; Voiry, D.; Chhowalla, M. Metallic 1T phase MoS2 nanosheets as supercapacitor electrode materials. *Nat. Nanotechnol.* **2015**, *10*, 313−318.

(18) Acerce, M.; Akdoan, E. K.; Chhowalla, M. Metallic molybdenum disulfide nanosheet-based electrochemical actuators. *Nature* **2017**, *549*, 370−373.

(19) Voiry, D.; Salehi, M.; Silva, R.; Fujita, T.; Chen, M.; Asefa, T.; Shenoy, V. B.; Eda, G.; Chhowalla, M. Conducting MoS2 nanosheets as catalysts for hydrogen evolution reaction. *Nano Lett.* **2013**, *13*, 6222−6227.

(20) Lukowski, M. A.; Daniel, A. S.; Meng, F.; Forticaux, A.; Li, L.; Jin, S. Enhanced hydrogen evolution catalysis from chemically exfoliated metallic MoS2 nanosheets. *J. Am. Chem. Soc.* **2013**, *135*, 10274−10277.

(21) Tang, Q.; Jiang, D. E. Mechanism of hydrogen evolution reaction on 1T-MoS2 from first principles. *ACS Catal.* **2016**, *6*, 4953−4961.

(22) Wang, D.; Zhang, X.; Bao, S.; Zhang, Z.; Fei, H.; Wu, Z. Phase engineering of a multiphasic 1T/2H MoS2 catalyst for highly efficient hydrogen evolution. *J. Mater. Chem. A* **2017**, *5*, 2681−2688.

(23) Liu, H.; Grasseschi, D.; Dodda, A.; Fujisawa, K.; Olson, D.; Kahn, E.; Zhang, F.; Zhang, T.; Lei, Y.; Branco, R. B. N.; et al. Spontaneous chemical functionalization via coordination of Au single atoms on monolayer MoS2. *Sci. Adv.* **2020**, *6*, No. eabc9308.

(24) Zhang, D.; Wu, J.; Li, P.; Cao, Y. Room-temperature SO2 gas-sensing properties based on a metal-doped MoS2 nanoflower: An experimental and density functional theory investigation. *J. Mater. Chem. A* **2017**, *5*, 20666−20677.

(25) Gao, B.; Zhao, Y.; Du, X.; Chen, Y.; Guan, B.; Li, Y.; Li, Y.; Ding, S.; Zhao, H.; Xiao, C.; Song, Z. Facile phase transition engineering of MoS2 for electrochemical hydrogen evolution. *J. Mater. Chem. A* **2021**, *9*, 8394−8400.

(26) Wang, C.; de Oliveira, R. F.; Jiang, K.; Zhao, Y.; Turetta, N.; Ma, C.; Han, B.; Zhang, H.; Tranca, D.; Zhuang, X.; et al. Boosting the electronic and catalytic properties of 2D semiconductors with supramolecular 2D hydrogen-bonded superlattices. *Nat. Commun.* **2022**, *13*, No. 510.

(27) Benson, E. E.; Zhang, H.; Schuman, S. A.; Nanayakkara, S. U.; Bronstein, N. D.; Ferrere, S.; Blackburn, J. L.; Miller, E. M. Balancing the hydrogen evolution reaction, surface energetics, and stability of metallic MoS2 nanosheets via covalent functionalization. *J. Am. Chem. Soc.* **2018**, *140*, 441−450.

(28) Kang, Y.; Najmaei, S.; Liu, Z.; Bao, Y.; Wang, Y.; Zhu, X.; Halas, N. J.; Nordlander, P.; Ajayan, P. M.; Lou, J.; Fang, Z. Plasmonic Hot Electron Induced Structural Phase Transition in a MoS2Monolayer. *Adv. Mater.* **2014**, *26*, 6467−6471.
(29) Butun, S.; Tongay, S.; Aydin, K. Enhanced Light Emission from Large-Area Monolayer MoS2 Using Plasmonic Nanodisc Arrays. *Nano Lett.* **2015**, *15*, 2700−2704.
(30) Miao, J.; Hu, W.; Jing, Y.; Luo, W.; Liao, L.; Pan, A.; Wu, S.; Cheng, J.; Chen, X.; Lu, W. Surface plasmon-enhanced photodetection in few layer MoS2 phototransistors with au nanostructure arrays. *Small* **2015**, *11*, 2392−2398.
(31) Wu, J.; Zeng, H.; Li, X.; Xiang, X.; Liao, Y.; Xue, Z.; Ye, Y.; Xie, X. Ultralight Layer-by-Layer Self-Assembled MoS2-Polymer Modified Separator for Simultaneously Trapping Polysulfides and Suppressing Lithium Dendrites. *Adv. Energy Mater.* **2018**, *8*, 1−12.
(32) Eksik, O.; Gao, J.; Shojaee, S. A.; Thomas, A.; Chow, P.; Bartolucci, S. F.; Lucca, D. A.; Koratkar, N. Epoxy nanocomposites with two-dimensional transition metal dichalcogenide additives. *ACS Nano* **2014**, *8*, 5282−5289.
(33) Zhang, H.; Koledin, T. D.; Xiang, W.; Hao, J.; Nanayakkara, S. U.; Attanayake, N. H.; Li, Z.; Mirkin, M. V.; Miller, E. M. Stabilizing the heavily-doped and metallic phase of MoS2monolayers with surface functionalization. *2D Mater.* **2022**, *9*, No. 015033.
(34) Han, B.; Zhao, Y.; Ma, C.; Wang, C.; Tian, X.; Wang, Y.; Hu, W.; Samorì, P. Asymmetric Chemical Functionalization of Top-Contact Electrodes: Tuning the Charge Injection for High-Performance MoS2 Field-Effect Transistors and Schottky Diodes. *Adv. Mater.* **2022**, *34* (12), No. 2109445.
(35) Guan, Q.; Yan, H.; Cai, Y. Flatten the Li-ion Activation in Perfectly Lattice-Matched MXene and 1T-MoS2 Heterostructures via Chemical Functionalization. *Adv. Mater. Interfaces* **2022**, *9* (7), No. 2101838.
(36) Chen, W. Y.; Yen, C. C.; Xue, S.; Wang, H.; Stanciu, L. A. Surface Functionalization of Layered Molybdenum Disulfide for the Selective Detection of Volatile Organic Compounds at Room Temperature. *ACS Appl. Mater. Interfaces* **2019**, *11*, 34135−34143.
(37) Lee, S.; Kang, Y.; Lee, J.; Kim, J.; Shin, J. W.; Sim, S.; Go, D.; Jo, E.; Kye, S.; Kim, J.; An, J. Atomic layer deposited Pt nanoparticles on functionalized MoS2 as highly sensitive H2 sensor. *Appl. Surf. Sci.* **2022**, *571*, No. 151256.
(38) Ries, L.; Petit, E.; Michel, T.; Diogo, C. C.; Gervais, C.; Salameh, C.; Bechelany, M.; Balme, S.; Miele, P.; Onofrio, N.; Voiry, D. Enhanced sieving from exfoliated MoS2 membranes via covalent functionalization. *Nat. Mater.* **2019**, *18*, 1112−1117.
(39) Liu, M.; Zhu, H.; Wang, Y.; Sevencan, C.; Li, B. L. Functionalized MoS2-based nanomaterials for cancer phototherapy and other biomedical applications. *ACS Mater. Lett.* **2021**, *3*, 462−496.
(40) Deng, J.; Li, H.; Xiao, J.; Tu, Y.; Deng, D.; Yang, H.; Tian, H.; Li, J.; Ren, P.; Bao, X. Triggering the electrocatalytic hydrogen evolution activity of the inert two-dimensional MoS2 surface via single-atom metal doping. *Energy Environ. Sci.* **2015**, *8*, 1594−1601.
(41) Yao, X.; Zhu, J.; Wang, H.; Yang, K.; Shu, Y.; He, J. Facile synthesis of Fe-MoS2/NRGO composite material as effective electrocatalyst for high-efficiency hydrogen evolution reaction. *Appl. Surf. Sci.* **2022**, *587*, No. 152842.
(42) Shi, Y.; Zhou, Y.; Yang, D. R.; Xu, W. X.; Wang, C.; Wang, F. B.; Xu, J. J.; Xia, X. H.; Chen, H. Y. Energy Level Engineering of MoS2 by Transition-Metal Doping for Accelerating Hydrogen Evolution Reaction. *J. Am. Chem. Soc.* **2017**, *139*, 15479−15485.
(43) Luo, Z.; Ouyang, Y.; Zhang, H.; Xiao, M.; Ge, J.; Jiang, Z.; Wang, J.; Tang, D.; Cao, X.; Liu, C.; Xing, W. Chemically activating MoS2 via spontaneous atomic palladium interfacial doping towards efficient hydrogen evolution. *Nat. Commun.* **2018**, *9*, No. 2120.
(44) Xiong, Q.; Wang, Y.; Liu, P. F.; Zheng, L. R.; Wang, G.; Yang, H. G.; Wong, P. K.; Zhang, H.; Zhao, H. Cobalt Covalent Doping in MoS2 to Induce Bifunctionality of Overall Water Splitting. *Adv. Mater.* **2018**, *30* (29), No. 1801450.
(45) Zhang, H.; Yu, L.; Chen, T.; Zhou, W.; Lou, X. W. D. Surface Modulation of Hierarchical MoS2 Nanosheets by Ni Single Atoms for Enhanced Electrocatalytic Hydrogen Evolution. *Adv. Funct. Mater.* **2018**, *28*, 1−8.
(46) Chen, J.; Li, F.; Tang, Y.; Tang, Q. Tuning the phase stability and surface HER activity of 1T'-MoS 2 by covalent chemical functionalization. *J. Mater. Chem. C* **2020**, *8*, 15852−15859.
(47) Ding, J.; Peng, Z.; Wang, Z.; Zeng, C.; Feng, Y.; Yang, M.; Hu, G.; Luo, J.; Liu, X. Phosphorus-tungsten dual-doping boosts acidic overall seawater splitting performance over RuOx nanocrystals. *J. Mater. Chem. A* **2024**, *12*, 28023−28031.
(48) Voiry, D.; Goswami, A.; Kappera, R.; Silva, C. d. C. C. e.; Kaplan, D.; Fujita, T.; Chen, M.; Asefa, T.; Chhowalla, M. Covalent functionalization of monolayered transition metal dichalcogenides by phase engineering. *Nat. Chem.* **2015**, *7*, 45−49.
(49) Voiry, D.; Chhowalla, M.; Gogotsi, Y.; Kotov, N. A.; Li, Y.; Penner, R. M.; Schaak, R. E.; Weiss, P. S. Best practices for reporting electrocatalytic performance of nanomaterials. *ACS Nano* **2018**, *12* (10), 9635−9638.
(50) Hohenberg, P.; Kohn, W. Inhomogeneous electron gas. *Phys. Rev.* **1964**, *136*, No. B864.
(51) Kohn, W.; Sham, L. J. Self-consistent equations including exchange and correlation effects. *Phys. Rev.* **1965**, *140*, No. A1133.
(52) Enkovaara, J.; Rostgaard, C.; Mortensen, J. J.; Chen, J.; Dułak, M.; Ferrighi, L.; Gavnholt, J.; Glinsvad, C.; Haikola, V.; Hansen, H.; et al. Electronic structure calculations with GPAW: a real-space implementation of the projector augmented-wave method. *J. Phys.: Condens. Matter* **2010**, *22*, No. 253202.
(53) Ihm, J.; Zunger, A.; Cohen, M. L. Momentum-space formalism for the total energy of solids. *J. Phys. C: Solid State Phys.* **1979**, *12*, 4409.
(54) Blöchl, P. E. Projector augmented-wave method. *Phys. Rev. B* **1994**, *50*, No. 17953.
(55) Perdew, J. P.; Burke, K.; Ernzerhof, M. Generalized gradient approximation made simple. *Phys. Rev. Lett.* **1996**, *77*, 3865.
(56) Caldeweyher, E.; Ehlert, S.; Hansen, A.; Neugebauer, H.; Spicher, S.; Bannwarth, C.; Grimme, S. A generally applicable atomic-charge dependent London dispersion correction. *J. Chem. Phys.***2019** *150*, 154122..
(57) Caldeweyher, E.; Mewes, J.-M.; Ehlert, S.; Grimme, S. Extension and evaluation of the D4 London-dispersion model for periodic systems. *Phys. Chem. Chem. Phys.* **2020**, *22*, 8499−8512.
(58) Monkhorst, H. J.; Pack, J. D. Special points for Brillouin-zone integrations. *Phys. Rev. B* **1976**, *13*, 5188.
(59) Nørskov, J. K.; Bligaard, T.; Logadottir, A.; Kitchin, J.; Chen, J. G.; Pandelov, S.; Stimming, U. Trends in the exchange current for hydrogen evolution. *J. Electrochem. Soc.* **2005**, *152*, J23.
(60) Eng, A. Y. S.; Ambrosi, A.; Sofer, Z.; Šimek, P.; Pumera, M. Electrochemistry of transition metal dichalcogenides: Strong dependence on the metal-to-chalcogen composition and exfoliation method. *ACS Nano* **2014**, *8*, 12185−12198.
(61) Ambrosi, A.; Sofer, Z.; Pumera, M. Lithium Intercalation Compound Dramatically Infl uences the Electrochemical Properties of Exfoliated MoS 2. *Small* **2015**, *11*, 605−612.
(62) Yu, Y.; Nam, G.-H.; He, Q.; Wu, X.-J.; Zhang, K.; Yang, Z.; Chen, J.; Ma, Q.; Zhao, M.; Liu, Z.; et al. High phase-purity 1T'-MoS2-and 1T'-MoSe2-layered crystals. *Nat. Chem.* **2018**, *10*, 638−643.
(63) Duerloo, K.-A. N.; Li, Y.; Reed, E. J. Structural phase transitions in two-dimensional Mo-and W-dichalcogenide monolayers. *Nat. Commun.* **2014**, *5*, No. 4214.
(64) Sim, D. M.; Han, H. J.; Yim, S.; Choi, M.-J.; Jeon, J.; Jung, Y. S. Long-Term Stable 2H-MoS2 Dispersion: Critical Role of Solvent for Simultaneous Phase Restoration and Surface Functionalization of Liquid-Exfoliated MoS2. *ACS Omega* **2017**, *2*, 4678−4687.
(65) Voiry, D.; Goswami, A.; Kappera, R.; Silva, C. D. C. C. E.; Kaplan, D.; Fujita, T.; Chen, M.; Asefa, T.; Chhowalla, M. Covalent functionalization of monolayered transition metal dichalcogenides by phase engineering. *Nat. Chem.* **2015**, *7*, 45−49.

https://doi.org/10.1021/acs.jpcc.4c05965
J. Phys. Chem. C 2024, 128, 20856−20865

(66) Benck, J. D.; Hellstern, T. R.; Kibsgaard, J.; Chakthranont, P.; Jaramillo, T. F. Catalyzing the hydrogen evolution reaction (HER) with molybdenum sulfide nanomaterials. *ACS Catal.* **2014**, *4*, 3957−3971.
(67) Li, P.; Jiang, Y.; Hu, Y.; Men, Y.; Liu, Y.; Cai, W.; Chen, S. Hydrogen bond network connectivity in the electric double layer dominates the kinetic pH effect in hydrogen electrocatalysis on Pt. *Nat. Catal.* **2022**, *5*, 900−911.

https://doi.org/10.1021/acs.jpcc.4c05965
J. Phys. Chem. C 2024, 128, 20856−20865